Revista Mexicana de Astronomía y Astrofísica, **47**, 49–61 (2011)

PLANETARY NEBULAE IN THE INNER MILKY WAY II: THE BULGE-DISK TRANSITION

O. Cavichia, R. D. D. Costa, and W. J. Maciel

Instituto de Astronomia, Geofísica e Ciências Atmosféricas
Universidade de São Paulo, Brazil

Received 2010 November 29; accepted 2011 January 14

RESUMEN

En este trabajo se usa una muestra de nebulosas planetarias localizadas en el disco interno y en el bulbo de la Galaxia con objeto de encontrar la distancia galactocéntrica que mejor separa estas dos poblaciones desde el punto de vista de las abundancias. Se utilizan escalas de distancias estadísticas para estudiar la distribución de abundancias en la interfase disco-bulbo. Mediante una prueba de Kolmogorov-Smirnov se encuentra la distancia a la cual las propiedades químicas de estas regiones mejor se separan.

El resultado del análisis estadístico indica que, en promedio, la población interior tiene menores abundancias que la exterior. Además, la población interior no sigue el gradiente radial del disco hacia el centro galáctico. Basados en nuestros resultados, sugerimos que la interfase disco-bulbo está situada a 1.5 kpc del centro, y marca la transición entre la población del bulbo y la del disco interno, definida como la población de masas intermedias.

ABSTRACT

In this work, a sample of planetary nebulae located in the inner-disk and bulge of the Galaxy is used in order to find the galactocentric distance which better separates these two populations, from the point of view of abundances. Statistical distance scales are used to study the distribution of abundances across the disk-bulge interface. A Kolmogorov-Smirnov test is used to find the distance at which the chemical properties of these regions better separate.

The results of the statistical analysis indicate that, on the average, the inner population has lower abundances than the outer. Additionally, for the α-element abundances, the inner population does not follow the disk radial gradient towards the galactic center. Based on our results, we suggest a bulge-disk interface at 1.5 kpc, marking the transition between the bulge and inner-disk of the Galaxy as defined by the intermediate mass population.

Key Words: Galaxy: abundances — Galaxy: evolution — planetary nebulae: general — techniques: spectroscopic

1. INTRODUCTION

Chemical abundances of Planetary Nebulae (PNe) are an important tool to investigate the chemical evolution of the Galaxy. As a final stage of evolution of low and intermediate-mass stars ($\sim$1–8 $M_\odot$), the abundances of α-elements found in PNe usually are not modified by the evolution of the progenitor star. In this sense, chemical abundances of PNe can be used to study the chemical evolution of galaxies as done by Maciel, Lago, & Costa (2005, 2006), Fu et al. (2009), Stanghellini & Haywood (2010).

The chemical abundances obtained from PNe are relatively accurate and the nebulae can be observed at large distances in the Galaxy, even in regions obscured by the dust in the galactic disk, since they have bright emission lines, such as [O III]λ500.7 nm and Hα. Therefore PNe are useful to study the pattern of abundances in the inner-disk and bulge of the

Galaxy, where the extinction in the optical range is very severe (see for example Escudero & Costa 2001; Escudero, Costa, & Maciel 2004; Chiappini et al. 2009; Cavichia, Costa, & Maciel 2010). On the other hand, PNe distances are still subject to discussion. Only in a few cases can the distances be determined by a direct method, such as for nearby PNe, which have the distances determined by trigonometric parallax, or in cases where there is a main sequence binary companion. In the cases were accurate individual distances cannot be determined, alternative methods have been developed in order to obtain reliable distances. In these cases, distances are derived from nebular properties (see e.g., Maciel & Pottasch 1980; Cahn, Kaler, & Stanghellini 1992; Stanghellini, Shaw, & Villaver 2008). These methods are called statistical methods and the distances so obtained are called statistical distances. In spite of the uncertainties, statistical distance scales are still the best tool to study the chemical abundance patterns in the Galaxy from the point of view of PNe, as done by Maciel & Quireza (1999), Maciel et al. (2006), Perinotto & Morbidelli (2006), and recently by Gutenkunst et al. (2008), Stanghellini & Haywood (2010), Henry et al. (2010).

From the point of view of the chemical evolution of the Galaxy, the bulge and the disk display different chemical abundance patterns such as the radial abundance gradients in the disk (Carigi et al. 2005; Daflon & Cunha 2004; Andrievsky et al. 2004; Maciel et al. 2005, 2006), or the wide abundance distribution in the bulge (Rich 1988; Zoccali et al. 2003, 2006). Also, the bulge and the disk may have different evolution histories, as described for example by the multiple infall scenario (Costa, Escudero, & Maciel 2005; Costa, Maciel, & Escudero 2008) or by the inside out formation model (Chiappini, Matteucci, & Romano 2001), respectively. As a consequence, we expect these differences to be reflected on the chemical properties of each component.

Additionally, the gas density, and consequently the star formation rate (SFR), also decrease in the inner Galaxy as found by Portinari & Chiosi (1999). They attribute this result to the influence of the galactic bar in the first 3 kpc of the Galaxy (see for example Gerhard 2002; Binney 2009). The decrease of the SFR is reflected on the α-element abundances in PNe, since a lower SFR limits the total mass ejected by the progenitor star, and consequently the chemical enrichment of the ISM decreases throughout the succeeding stellar generations. The galactic evolution models also point to a severe decrease in the SFR and chemical abundances at radii smaller than 3 kpc (Portinari & Chiosi 2000). Other chemical evolution models also predict a flatter abundance gradient in the inner-disk, such as those by Hou, Prantzos, & Boissier (2000) and Mollá & Díaz (2005).

Some recent work seems to support this scenario, based on the fact that towards the galactic center, stars do not follow the chemical abundance gradient found in the disk (Cunha et al. 2007). Davies et al. (2009) studying the chemical abundance patterns of the Scutum red supergiant clusters, located at the end of the galactic bar, find that there is a minimum in the abundances in this region, compared to other azimuthal angles.

From the point of view of PNe, the results of Gutenkunst et al. (2008) also point to a discontinuity in the abundance gradient towards the galactic center, in the sense that the abundances of bulge PNe do not follow the trend of those from the disk, as can be seen in their Figure 4. Górny et al. (2004) also notice that the oxygen gradient of the PNe population in the galactic disk flattens in the most internal parts of the Galaxy, and may even change sign. On the other hand, Chiappini et al. (2009) compared the abundances of PNe located in the bulge, inner-disk and Large Magellanic Cloud. Their results do not show any clear difference between bulge and inner-disk objects.

Other previous studies of the galactic bulge based on abundances of PNe such as Ratag et al. (1992), Cuisinier et al. (2000), Escudero & Costa (2001), Escudero et al. (2004), Exter, Barlow, & Walton (2004), find that bulge PNe have an abundance distribution similar to disk PNe, showing that He, O, Si, Ar, and Ca have a normal abundance pattern, and favoring therefore a slower galactic evolution than that indicated by stars. In conclusion, the distribution of chemical abundances in the inner region of the Galaxy is still an open question, especially regarding the bulge-disk connection. On the other hand, a detailed comparison of the bulge and inner-disk populations is important in order to characterize the galactic bulge as a "pseudobulge", as suggested by photometric and kinematic evidences (Howard et al. 2009; Shen et al. 2010), in opposition to a classical bulge as suggested by Binney (2009).

Both from modelling and from observational results, we expect a galactocentric distance to exist which better separates the populations of the bulge and inner-disk from the point of view of chemical abundances. However, such transition is still to be determined from the point of view of chemical abundances. The goal of this paper is to perform a statistical analysis using the new data provided by Cavichia et al. (2010, hereafter Paper I), and additional data from the literature, in order to characterize the interface between the bulge and inner-disk of the Galaxy, as defined by the PNe population. Taking into account both the abundance distributions and the individual distances for a sample of PNe, we are able to characterize the interface by establishing at which galactocentric distance bulge and disk characteristics better separate.

This paper is organized as follows: in § 2 the details of the sample and the new distances to our objects are presented. In § 3 the method used in order to characterize the bulge-disk transition is described. In § 4 we discuss the results and compare them with other results in the literature. Finally, in § 5 the main conclusions are presented.

2. THE SAMPLE AND NEW DISTANCES

2.1. *The Sample*

An extensive number of statistical scales have been proposed in the literature, and two of them have been adopted in order to study the chemical abundance distribution in the inner Galaxy: the Stanghellini et al. (2008, hereafter SSV08), and the Zhang (1995, hereafter Z95), distance scales. These scales are based on the Shklovsky method but with the introduction of a relationship between the ionized mass and the radius of the nebula, as proposed by Maciel & Pottasch (1980). SSV08 is a recent revision of the Cahn et al. (1992, hereafter CKS92), scale based on the physical properties of the PNe in the Magellanic Clouds, whose distances are accurately known. As the authors argue, this new distance scale is the most reliable to date.

The selection criteria applied to search for objects in the two catalogues (SSV08 and Z95) were the following: we selected those PNe which had 5 GHz fluxes lower than 100 mJy, optical diameters smaller than 12 arcsec, and galactic coordinates within the range $|\ell| \leq 10°$ and $|b| \leq 10°$. The galactic coordinates were used to take into account only the PNe which are in the galactic center direction. The combination of the other two criteria leads to the rejection of about 90–95% of the PNe which are in the galactic center direction, but have heliocentric distances of less than 4 kpc (cf. Stasińska, Richer, & McCall 1998). These criteria are commonly used by other authors to select bulge PNe (e.g., Exter et al. 2004 and Chiappini et al. 2009), so that most of the objects considered in this work should be at or near the bulge.

In order to study the chemical abundance distribution in the inner Galaxy, we have made use of the data published by our group (Cavichia et al. 2010; Escudero et al. 2004; Escudero & Costa 2001). We also searched for chemical abundances of PNe located in the bulge and inner-disk of the Galaxy in the following works: Ratag et al. (1997), Exter et al. (2004), Górny et al. (2004), Perinotto, Morbidelli, & Scatarzi (2004), de Freitas Pacheco, Maciel, & Costa (1992), Köppen, Acker, & Stenholm (1991), Samland et al. (1992), Cuisinier et al. (2000). All these works deal with the same region of interest, and, besides that, they contain significant and homogeneous samples, which is very important in multi-object study, as we propose in this work. For more details on these works see Paper I. Adding these objects to our original sample in Paper I, our database contains 140 objects, as given in Table 1. In this table, the columns give the PN G number, the name of the nebula, the galactocentric distance in kpc for the SSV08 and the Z95 distance scales, respectively. An asterisk marks those PNe whose distances were derived in the present work. The galactocentric distances of the objects located beyond the galactic bulge are given with a negative sign in Table 1. The extinction in this region is very high, and the uncertainties in the distances are large, reaching 30% in some cases. For example, an object with a heliocentric distance of 8 kpc in this direction according to both scales will have a true heliocentric distance between 5.6 and 10.4. Therefore, it is unlikely that these objects are really located far beyond the galactic bulge, so that we assume that they actually belong to the bulge population. The implications of this assumption will be further discussed in § 3.3. More details on the new distances and the determination of the galactocentric distances are given in § 2.2.

2.2. *New distances to the Planetary Nebulae*

Several of the objects for which the chemical abundances were determined in Paper I, do not have distances published by SSV08. In order to include these PNe in our analysis, their distances were estimated from equations (8a) and (8b) of SSV08. In cases where the 5 GHz flux was not available, their equivalent 5 GHz flux from Hβ flux was derived using equation (6) in CKS92. The optical thickness parameter was derived from equation (2) in SSV08. Angular radii were obtained from the literature, most of them from Acker et al. (1992), and some from more recent works such as Tylenda et al. (2003) and Ruffle et al. (2004). The objects with new distances are marked with an asterisk in Table 1, and the data

TABLE 1

GALACTOCENTRIC DISTANCES OF PNE IN THE SAMPLE

PN G	Name	R_{SSV08} (kpc)	R_{Z95} (kpc)	PN G	Name	R_{SSV08} (kpc)	R_{Z95} (kpc)
000.1–01.1	M3-43	–	1.81	009.4–09.8	M3-32	1.85	1.57
000.2–01.9	M2-19	−0.30	0.63	009.6–10.6	M3-33	−1.45	–
000.3–04.6	M2-28	–	−0.70	009.8–04.6	H1-67	0.64	0.80
000.4–02.9	M3-19	0.31	−0.73	010.4+04.5	M2-17	–	0.85
000.7–02.7	M2-21	−2.20	–	010.7–06.4	IC4732	1.51	3.22
000.7–03.7	M3-22	0.50	−0.63	010.7–06.7	Pe1-13	−1.37	–
000.7+03.2	Hen 2-250	–	1.07	010.7+07.4*	Sa2-230	1.41	–
000.9–04.8	M3-23	3.78	3.45	010.8–01.8	NGC 6578	4.42	–
001.0+01.9	K1-4	6.06	–	011.0+05.8	NGC 6439	1.89	–
001.2–03.0	H1-47	–	−2.07	350.5–05.0*	H1-28	−1.93	–
001.2+02.1	Hen 2-262	−1.57	1.39	350.9+04.4	H2-1	2.45	–
001.4+05.3	H1-15	−1.29	0.73	351.1+04.8	M1-19	−2.75	0.71
001.7–04.6	H1-56	–	−3.06	351.2+05.2	M2-5	–	0.80
001.7+05.7	H1-14	1.73	2.24	351.6–06.2*	H1-37	−1.81	–
002.0–02.0*	H1-45	−7.12	−0.36	352.0–04.6	H1-30	–	2.88
002.0–06.2	M2-33	−1.09	−1.02	352.1+05.1	M2-8	−1.39	1.05
002.1–02.2	M3-20	0.44	2.71	352.6+03.0	H1-8	−0.91	–
002.1–04.2	H1-54	−4.39	−0.57	353.7+06.3	M2-7	1.19	−1.00
002.2–02.7	M2-23	3.75	−0.51	354.2+04.3	M2-10	–	−2.73
002.2–09.4	Cn1-5	2.83	3.70	355.1–02.9	H1-31	–	−3.78
002.4+05.8	NGC 6369	6.92	–	355.1–06.9	M3-21	–	2.55
002.6–03.4	M1-37	–	−0.62	355.4–02.4	M3-14	2.33	1.58
002.6+08.1	H1-11	1.19	1.30	355.4–04.0	Hf2-1	1.92	–
002.7–04.8	M1-42	2.53	3.15	355.7–03.0	H1-33	−4.05	−1.23
002.7+01.6	H2-20	–	0.53	355.7–03.4*	H1-35	2.15	2.03
002.8–02.2	Pe2-12	–	−4.12	355.9–04.2	M1-30	–	2.18
003.1+02.9	Hb4	2.98	–	355.9+03.6*	H1-9	2.19	–
003.1+03.4	H2-17	–	−0.98	356.2–04.4	Cn2-1	−0.56	1.91
003.2–06.1	M2-36	2.03	1.29	356.3–06.2*	M3-49	−5.33	–
003.3–04.6	Ap1-12	3.42	–	356.5–02.3	M1-27	3.41	4.27
003.4–04.8	H2-43	–	3.03	356.5–03.9	H1-39	−7.28	−2.08
003.5–04.6	NGC 6565	3.37	3.68	356.7–04.8	H1-41	2.37	1.51
003.6–02.3	M2-26	−0.40	−1.46	356.8–05.4*	H2-35	1.86	–
003.7–04.6	M2-30	−1.55	−0.68	356.9–05.8	M2-24	−1.52	−3.86
003.8–04.3	H1-59	−1.53	−3.18	356.9+04.4	M3-38	−6.07	−0.65
003.8–04.5	H2-41	−0.85	−6.23	356.9+04.5	M2-11	–	1.08
003.8+05.3	H2-15	−7.40	−8.96	357.1–04.7	H1-43	−5.33	−3.59
003.9–02.3	M1-35	1.93	3.38	357.1+03.6	M3-7	1.73	2.62
004.0–03.0	M2-29	−0.75	−2.01	357.2–04.5	H1-42	1.94	3.22
004.0–05.8	Pe1-12	1.66	−2.33	357.2+07.4	M4-3	–	−0.37
004.1–04.3	H1-60	−2.24	−0.82	357.3+03.3	M3-41	–	3.87
004.6+06.0	H1-24	–	0.89	357.3+04.0	H2-7	–	−1.32
004.8–05.0	M3-26	0.82	−0.82	357.4–03.2	M2-16	1.05	2.18
004.8+02.0	H2-25	−3.45	−4.22	357.4–03.5	M2-18	−7.74	−1.48
004.9+04.9	M1-25	1.50	3.11	357.4–04.6	M2-22	−0.79	−1.97
005.0+04.4	H1-27	0.65	−2.94	357.5+03.2	M3-42	1.17	−1.78
005.2+05.6	M3-12	–	1.24	357.6+01.7	H1-23	−1.74	1.89
005.5–02.5*	M3-24	1.34	–	357.6+02.6	H1-18	–	0.72
005.7–05.3	M2-38	1.24	−1.01	357.9–05.1	M1-34	–	2.15
005.8–06.1	NGC 6620	−1.19	1.61	358.2+03.5	H2-10	−5.35	−0.50
005.8+05.1	H2-16	2.81	–	358.2+03.6	M3-10	−1.40	1.72
006.0–03.6	M2-31	–	3.14	358.2+04.2	M3-8	0.96	0.78
006.1+08.3*	M1-20	−1.12	2.34	358.3–02.5	M4-7	1.66	2.81
006.4–04.6*	Pe2-13	1.92	–	358.3+03.0*	H1-17	0.42	−0.59
006.4+02.0	M1-31	2.94	4.10	358.5–04.2*	H1-46	−0.75	1.04
006.8–03.4*	H2-45	1.89	–	358.6+01.8	M4-6	–	1.76
006.8+04.1	M3-15	–	3.94	358.6+07.8	M3-36	–	−6.05
007.0–06.8	VY2-1	0.86	2.57	358.7–05.2*	H1-50	−3.03	0.79
007.0+06.3*	M1-24	−1.00	–	358.8+03.0	Th3-26	0.66	–
007.1–06.0	H1-66	–	−1.70	358.9+03.2	H1-20	0.64	2.91
007.2+01.8*	Hb6	3.78	–	358.9+03.3*	H1-19	−2.95	−0.51
007.5+07.4	M1-22	–	−4.02	359.1–01.7	M1-29	–	4.70
007.8–04.4	H1-65	–	−2.25	359.1–02.3	M3-16	1.30	1.50
008.0+03.9	NGC 6445	6.64	–	359.3–03.1	M3-17	−3.60	−1.10
008.1–04.7	M2-39	−4.02	−2.21	359.4–03.4	H2-33	0.54	−1.78
008.2–04.8	M2-42	−1.48	0.66	359.7–02.6	H1-40	0.84	0.36
008.2+06.8*	Hen 2-260	−12.23	−3.62	359.8+03.7	Th3-25	-6.52	–
008.3–07.3*	NGC 6644	2.18	4.01	359.8+06.9	M3-37	−8.69	−5.50
009.0+04.1	Th4-5	–	1.69	359.9–04.5	M2-27	−4.45	2.68
009.4–05.0	NGC 6629	5.67	–	359.9+05.1	M3-9	4.70	–

TABLE 2

NEW DISTANCES

PN G	Name	θ (arcsec)	F (mJy)	τ	d (kpc)
002.0–02.0	H1-45	0.8	20	2	15.1
005.5–02.5	M3-24	5.1	4.9	4.3	6.7
006.1+08.3	M1-20	0.8	50	1.7	8.1
006.4-04.6	Pe2-13	6.6	3.4	4.7	6.2
006.8–03.4	H2-45	4.6	9.7	3.9	6.2
007.0+06.3	M1-24	3.2	6.2	3.8	8.5
007.2+01.8	Hb6	2.5	240	2	4.3
008.2+06.8	Hen 2-260	0.5	10	1.9	20.4
008.3–07.3	NGC6644	1.3	100	1.8	6.1
010.7+07.4	Sa2-230	5	4	4.4	7.1
350.5–05.0	H1-28	3.9	1.5	4.6	9.9
351.6–06.2	H1-37	4.3	1.3	4.7	9.7
355.7–03.4	H1-35	1	90	1.7	5.9
355.9+03.6	H1-9	3.5	30	3.2	5.9
356.3–06.2	M3-49	4.9	0.2	5.7	13.2
356.8–05.4	H2-35	5.4	0.9	5.1	9.1
358.3+03.0	H1-17	0.5	40	1.4	7.9
358.5–04.2	H1-46	0.6	40	1.5	8.5
358.7–05.2	H1-50	0.7	30	1.8	10.9
358.9+03.3	H1-19	0.7	30	1.9	10.9

used in the determination are shown in Table 2. In this table, Column 1 gives the PN G number, Column 2, the name, Column 3, the angular diameter, Column 4, the 5 GHz flux, Column 5, the optical thickness parameter, and Column 6 lists the new distances derived for these objects.

2.3. *Galactocentric distances and distribution*

Heliocentric distances were converted into galactocentric distances using equation 1, where d is the heliocentric distance, b and ℓ the galactic latitude and longitude, respectively, and R_0 the solar distance to the galactic center. In this work we adopted $R_0 = 8$ kpc, as suggested by recent studies (Gillessen et al. 2009; Nishiyama et al. 2006).

$$R = \sqrt{R_0^2 + (d\cos\ b)^2 - 2\ R_0\ d\cos\ b\cos\ \ell}, \quad (1)$$

In order to check the distribution of distances for the PNe in our database, Figure 1 shows the distribution of the PNe with respect to the galactocentric distance for both distance scales used in this work, Z95 (left) and SSV08 (right), including the new distances derived in this work. The figure also shows a Gaussian fit to each histogram. The mean and standard deviation are (0.6 ± 0.3) kpc and (2.6 ± 0.3) kpc for the SSV08 scale, and (0.6 ± 0.2) kpc and (2.5 ± 0.2) kpc for the Z95 scale. For both scales, the mean is consistent with the most recent determinations of the solar distance to the galactic center, which are all near 8 kpc, while the widths are larger than the standard deviation expected of 1.2 kpc for the bulge. As discussed by Z95, this dispersion is a convolution of the probably real Gaussian distribution of the bulge, with the extra spread introduced by the mass-radius relationship.

3. DETERMINATION OF THE BULGE-DISK INTERFACE

3.1. *Abundance differences between bulge and inner-disk PNe*

In order to study the chemical abundance distribution in the inner Galaxy and to determine the bulge-disk interface, we made use of a method similar to that suggested by Maciel et al. (2006). First, a galactocentric distance (R_L) is chosen, which defines a limit for the sample. Then the sample is divided into two groups: Group I is composed by PNe with galactocentric distances smaller than the limit previously settled, and Group II, is composed by PNe with galactocentric distances larger than this limit. For each group, the average abundances and the standard error of the mean are calculated for the available elements, namely He, O, N, S, and Ne. Then, the limiting radius R_L is varied, considering distances in the interval from 0.1 to 3.6 kpc, in 0.7 kpc steps for each distance scale.

The results are shown in Figures 2 and 3 for the SSV08 and Z95 distance scales, respectively. In each figure, Group I is represented by filled circles joined by continuous lines and Group II by squares joined by dashed lines. Each pair of circle/square points in each plot represents the average abundance for that element adopting a given limit for the bulge-disk interface, as a function of the limiting distance. Therefore, each plot shows how the differences between the groups evolve adopting distinct limits to define them. Considering elements heavier than He, it can be seen that, on average, abundances of Group I are lower than those of Group II objects for both distance scales. That is, in most cases the objects of Group I, which are closer to the galactic center, have systematically lower abundances compared with the objects of Group II, for all chosen values of the limiting radius (R_L). The main exceptions are the helium abundances for both distance scales and argon for the Z95 scale, which present similar distributions for both groups. In the case of helium, these results are not surprising, as (a) this element is equally contaminated by the PN progenitor stars, both in the bulge

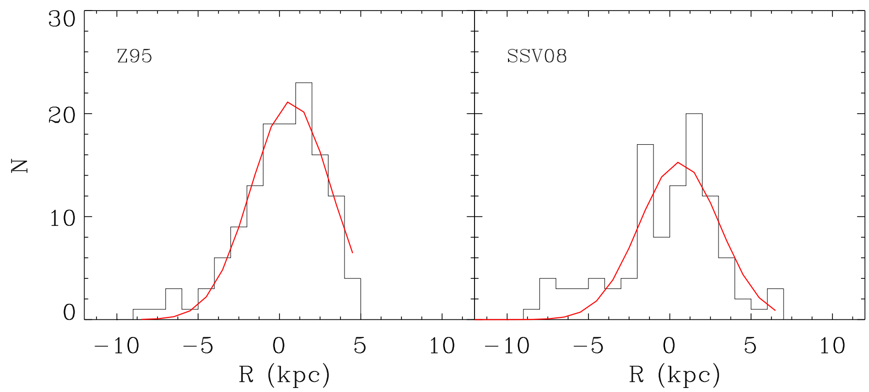

Fig. 1. Galactocentric distance distribution for the Z95 distance scale (left) and for the SSV08 distance scale (right). For each histogram a Gaussian fit is shown (see the text for more details).

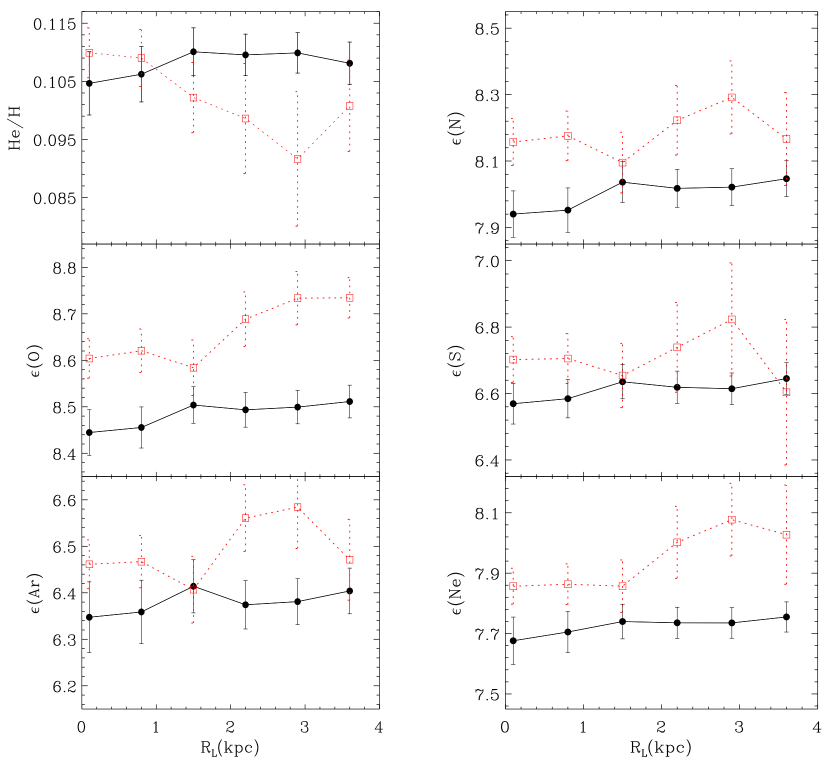

Fig. 2. Average abundances of PNe of Group I (circles joined by continuous lines) and Group II (squares joined by dashed lines) for the SSV08 distance scale. The abscissa gives the limiting galactocentric distance R_L, considered to be in the range 0–4 kpc. Error bars indicate the standard error of the mean for each subsample.

and in the galactic disk, and (b) helium does not show any measurable radial abundance gradient, in contrast with the remaining elements considered in this paper. (See a detailed discussion of the helium gradient in Maciel 2000).

Examining Figure 2 we see that for the α-elements oxygen, sulfur and argon the differences between both samples reach a minimum between 1.5 and 2.5 kpc, where it is of the order of 0.1 dex or lower. In Figure 3, examining now the α-elements, we see that a minimum difference appears around 1.5 or 2 kpc. For neon, the abundance difference between the groups is of the order of 0.2 dex, while for the other elements this difference is of the order

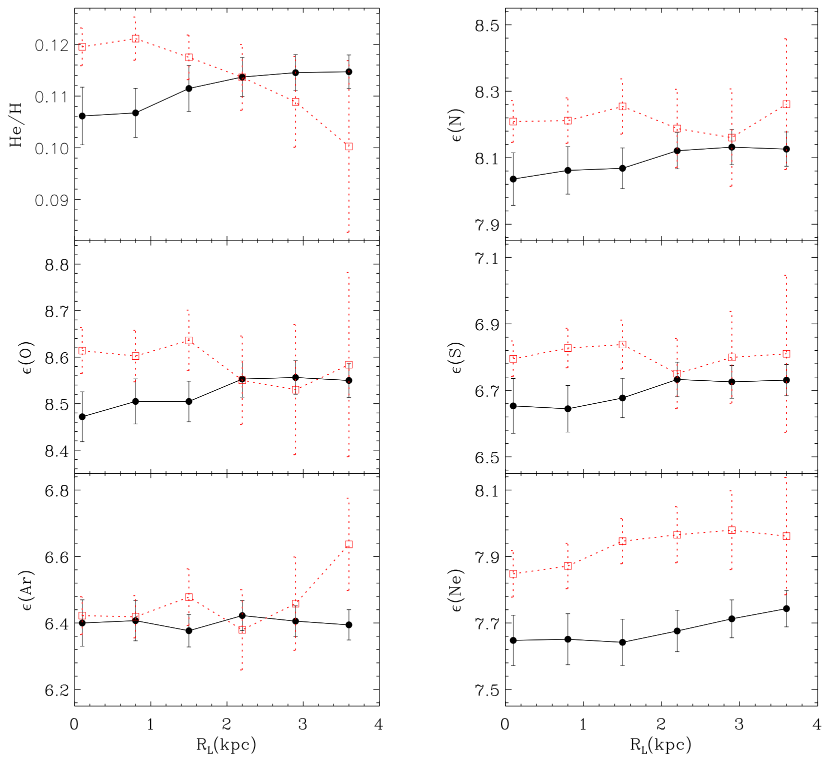

Fig. 3. The same as Figure 2 for the Z95 scale.

of 0.15 dex. For argon this difference is not clear, which is already expected since the ionization correction factor used to derive its abundance can lead to uncertainties larger than those for other elements.

3.2. *Kolmogorov-Smirnov test*

Our goal in this section is to find the distance that best characterizes the separation of the two groups, in the sense that the populations of each group should be as distinct as possible. In this case, we will be able to ascertain a value for the galactocentric distance of the bulge-disk interface based on the intermediate mass population represented by the PNe sample. In order to find such distance, we performed a Kolmogorov-Smirnov test for Groups I and II at each step of the procedure described above. The test returns the probabilities that the two groups are drawn from the same distribution. Small probabilities show that the cumulative distribution function of Group I is significantly different from Group II. The results are displayed in Figure 4. For each element the probability is shown as function of the limiting distance R_L. For each distance step, the left filled bar represents the SSV08 scale and the right empty bar the Z95 scale. Since we are looking for small probabilities, we can see from the figure that the lowest probabilities are achieved at 1.5 kpc for the Z95 distance scale for the elements O, S, Ar, and Ne. The probabilities for each element and distance are listed in Table 3 and the lowest values are highlighted in black. Again, it is clear that for the Z95 distance scale the lowest probabilities are achieved at 1.5 kpc for all the α-elements. On the other hand, SSV08 does not show a unique distance for the lowest probabilities. Indeed, considering only the α-elements, no distances are alike. Nevertheless, examining Figure 2 in detail, we can see that there is a step in the abundance radial distributions for the α-elements concerning the distance of 2.2 kpc. So that the safest conclusion we can draw is that $R_L < 2.9$ kpc based on the SSV08 distance scale.

3.3. *Resulting abundance distributions*

Adopting the separation distances obtained for each element and distance scale, namely 1.5 kpc for Z95 and 2.2 kpc for SSV08, the distribution of the abundances for each group are shown in Figures 5 and 6 for the Z95 and SSV08 distance scales, respectively. Empty histograms represent Group I objects, while filled histograms represent Group II objects. The number of objects used is also given for each plot.

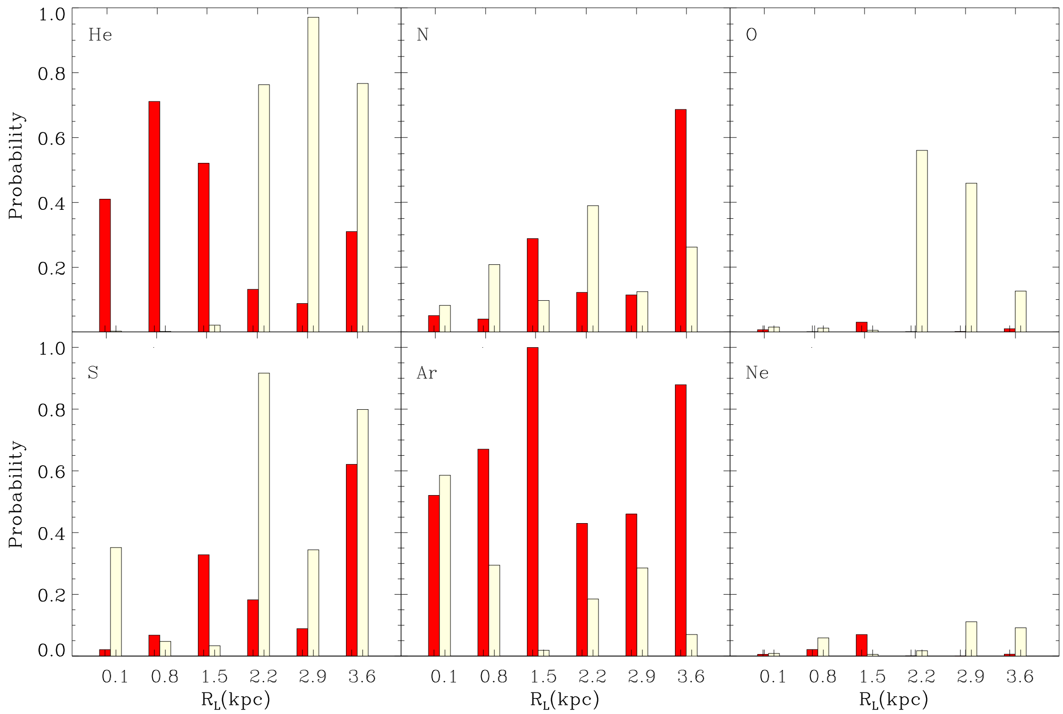

Fig. 4. Kolmogorov-Smirnov probability bar plot for each element as a function of the limiting radius of Groups I and II. Left filled bars correspond to the SSV08 scale and empty right bars to the Z95 scale.

TABLE 3

KOLMOGOROV-SMIRNOV PROBABILITIES

	$P(R_L)$ SSV08						$P(R_L)$ Z95					
R_L (kpc)	0.1	0.8	1.5	2.2	2.9	3.6	0.1	0.8	1.5	2.2	2.9	3.6
He	0.574	0.865	0.379	0.118	**0.080**	0.293	0.003	**0.0026**	0.022	0.763	0.971	0.767
N	**0.053**	0.075	0.335	0.103	0.099	0.647	**0.0819**	0.208	0.097	0.390	0.124	0.262
O	0.014	**0.001**	0.058	**0.001**	**0.001**	0.008	0.015	0.012	**0.0051**	0.560	0.459	0.126
S	**0.022**	0.074	0.370	0.154	0.077	0.583	0.352	0.047	**0.0334**	0.917	0.344	0.799
Ar	0.720	0.864	0.989	**0.394**	0.508	0.845	0.586	0.295	**0.0188**	0.185	0.285	0.070
Ne	0.014	0.046	0.128	0.001	**0.000**	0.007	0.009	0.059	**0.0056**	0.017	0.111	0.092

In Figure 5 the oxygen distribution for Group I is wider than that for Group II, while most objects from Group II have abundances centered at 8.5 dex. The other α-elements also show this pattern according to which Group II objects favor higher abundances than those from Group I. However, these differences are not larger than the individual errors in abundances. Among the α-elements, neon displays the largest difference between the two distributions. Nevertheless, some caution must be taken here. In a recent study by Milingo et al. (2010), there are some evidences that neon enhancement is present in a significant portion of PNe. This enhancement could be explained considering the charge exchange reaction $O^{++} + H^0 \rightarrow O^+ + H^+$ (see Peimbert, Luridiana, & Torres-Peimbert 1995, and references therein). Since the neon ICF depends inversely on the O^{++} abundance, the charge exchange reaction could increase the neon elemental abundance. If the neon enhancement is real, it does not represent the abundance of the interstellar medium at the time of the formation of the progenitor star. Thus, the neon distribution in Figure 5 must be interpreted carefully.

In Figure 6, showing the distribution of the abundances for the SSV08 scale, the oxygen distribution for Group I objects is wider than for Group II and the

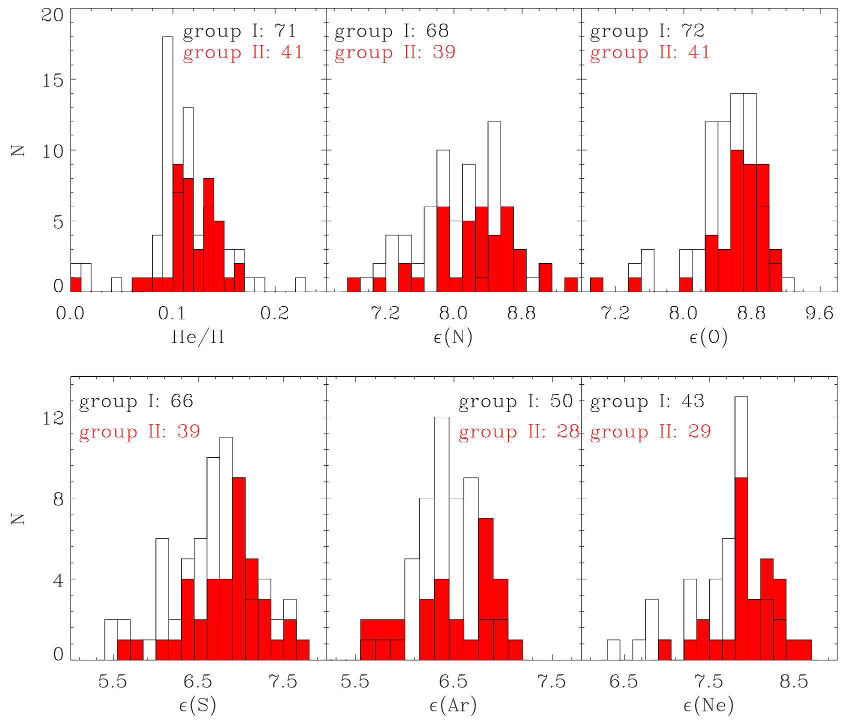

Fig. 5. Abundance distributions for Groups I and II using the Z95 distance scale. Unfilled histograms represent Group I objects and filled histograms are for Group II. The number of objects in each distribution is shown at the top.

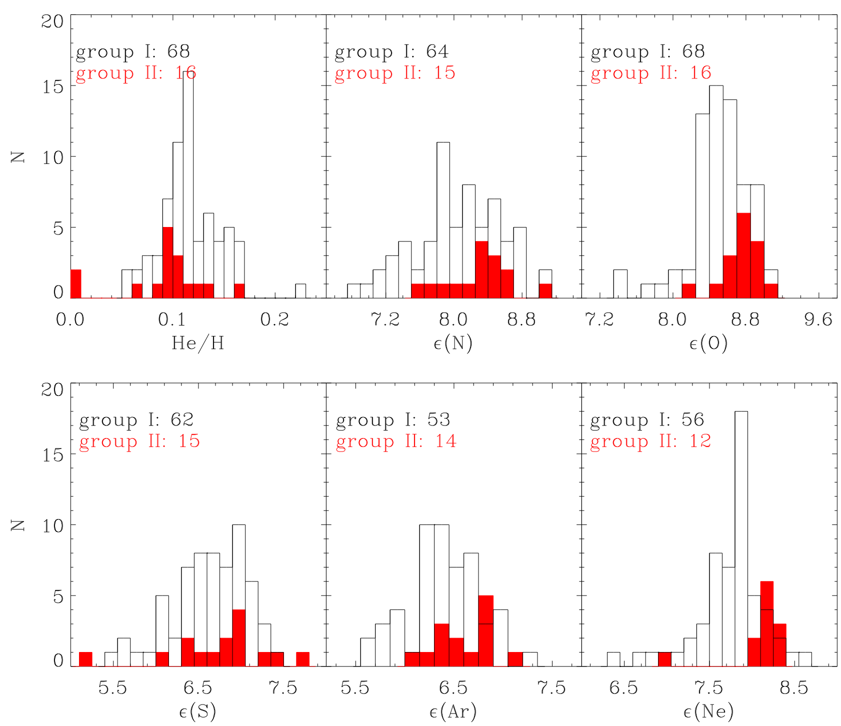

Fig. 6. The same as Figure 5 for the SSV08 distance scale.

TABLE 4

AVERAGE ABUNDANCES OF GROUPS I AND II FOR EACH DISTANCE SCALE

	SSV08		Z95	
Element	Group I	Group II	Group I	Group II
He/H	0.110 ± 0.004	0.099 ± 0.009	0.111 ± 0.004	0.117 ± 0.004
ϵ(N)	8.02 ± 0.06	8.22 ± 0.10	8.07 ± 0.06	8.25 ± 0.08
ϵ(O)	8.49 ± 0.04	8.69 ± 0.06	8.50 ± 0.04	8.64 ± 0.07
ϵ(S)	6.62 ± 0.05	6.74 ± 0.14	6.68 ± 0.06	6.84 ± 0.07
ϵ(Ar)	6.37 ± 0.05	6.56 ± 0.07	6.38 ± 0.05	6.48 ± 0.08
ϵ(Ne)	7.74 ± 0.05	8.00 ± 0.12	7.64 ± 0.07	7.95 ± 0.07

values are between 8.0 and 9.3 dex. The same trend is seen in the distributions for the SSV08 scale when compared with the Z95 scale: compared to Group I objects, the α-element distributions for Group II show a tendency to higher abundances.

Table 4 shows the average abundances and the standard error of the mean for Group I and II objects, adopting the distances 1.5 and 2.2 kpc for the Z95 and SSV08 scales as the limit between the two groups. Although these abundances are similar, reflecting the large dispersion of abundances found in these regions of the Galaxy, some important differences are apparent. In particular, the N, O, S, Ar, and Ne abundances are *smaller* for Group I compared to Group II for both distance scales. For N and O the difference between the two groups is 0.20 dex. For S, Ar, and Ne it is 0.12, 0.19 and 0.26 dex, respectively. In spite of the fact that these differences are not larger than the individual errors in the abundances, we can draw important conclusions about these results. The standard error of the mean is small since both groups have several objects and therefore the difference between both groups is statistically significant. This can be seen considering the lower and upper 90% and 68% confidence limits of each group. Although there are some overlaps between the distributions, for N, O, Ar, and Ne they are statistically significantly different considering the 68% confidence limit of each group for the SSV08 distance scale. Only the S distributions are not statistically different considering this method. For the Z95 distance scale, the distributions of N, O, and S of each group are significantly different considering the same confidence limit. The Ne distributions are statistically different considering the 90% confidence limit for this scale. These results are an important indication that bulge nebulae (Group I) do not follow the trends observed in the inner-disk (Group II), as we will discuss in § 4.

Relaxing the assumption that objects with adopted negative galactocentric distances belong to the bulge would not change the derived conclusions. We performed some tests excluding these objects, and the main conclusions are unchanged: bulge objects have lower α-element abundances than those in the inner disk. Adopting positive distances for these objects makes the group separation less clear, as the mixing of both populations is enhanced, but even in this case bulge objects still have lower abundances compared to inner disk objects.

The galactocentric distance of 1.5 kpc for the Z95 distance scale marks the limit at which the Groups I and II are more likely to separate from the point of view of the chemical abundances, as shown by the Kolmogorov-Smirnov test. On the other hand, the galactocentric distance of 2.2 kpc for the SSV08 scale was chosen from eye inspection in the radial abundances distributions, marking the limit in the α-elements abundances. In this case too, objects from Group II, whose galactocentric distances are greater than 2.2 kpc, have higher abundances than those from Group I, whose distances are lower than this limit.

Since the bulge and the disk display different chemical abundance characteristics, such as for example the radial abundance gradients found in the disk, or the large abundance distribution found in the bulge, as we discussed in § 1, we expect the existence of a galactocentric distance which better separates the two populations. Our analysis point to a separation at $R_L = 1.5$ kpc for the Z95 distance scale and $R_L < 2.9$ kpc for the SSV08 scale. Therefore, we can assign to Group I those objects that pertain to the bulge, and to Group II those that pertain to the inner-disk.

4. DISCUSSION

There are other evidences that point to a transition from the bulge to the inner-disk at a galactocentric distances similar to the distances found in this work. Indeed, infrared observations of the bulge, like those from the COBE/DIRBE satellite (Weiland et al. 1994), support these results. From their Figure 1, it is clear that the nuclear radius of the bulge is between $10°$ and $15°$. For the canonical solar distance to the galactic center of 8 kpc adopted in this work, the bulge longer radius is between 1.4 and 2.1 kpc.

From the point of view of giant stars, Tiede & Terndrup (1999) performed photometric and spectroscopic observations of 503 stars in four windows toward the bulge, with coordinates (ℓ,b) of ($-28.8°$,$-6°$), ($-8.7°$,$6.0°$), ($8.4°$,$-6.0°$) and ($24.4°$, $6.1°$). According to their results, the abundance distribution in the inner Galaxy presents a discontinuity. The authors argue that such a difference is larger than any bias in the sample selection and not due to errors in the abundances. As we are suggesting, they assign the difference found to the different populations in the line of sight.

Smartt et al. (2001) observed type-B stars located between 2.5 and 5 kpc from the galactic center. Due to the young nature of these stars, their photospheric abundances reflect the present day abundances of the ISM. Their results agree with ours in the sense that the oxygen abundance decreases for distances smaller than 3 kpc, as can be seen from their Figure 3. However, the error bars are large and it is only possible to say that the oxygen abundances do not follow the radial gradient of the disk toward the galactic center, since they are 0.3 to 0.4 dex lower than what we expected from the Rolleston et al. (2000) radial gradient, given their position.

In the light of recent studies using PNe, Gutenkunst et al. (2008) point to a discontinuity in the abundance gradient towards the galactic center, in the sense that the abundances of bulge PNe do not follow the trend of those from the disk, as can be seen in their Figure 4. The same trend can be seen in Figure 3 of Stanghellini & Haywood (2010). Considering PNe type III as defined by Peimbert (1978), which represent the old disk population, it is possible to note from their figure that oxygen abundances are smaller for galactocentric distances of less than 4 kpc.

Finally, Mishurov, Lépine, & Acharova (2002) proposed a galactic formation model where the spiral arms are inductors of stellar formation and they can exist only between the internal and external Lindblad resonances. As a consequence, the SFR decreases strongly outside these limits, and the chemical abundances are depleted in these regions. Combining these evidences with our results, we can point out to a bulge-disk interface for the intermediate mass population, marking therefore the transition between the disk and the bulge populations, at a galactocentric distance of 1.5 for the Z95 distance scale. On the other hand, for the SSV08 distance scale the Kolmogorov-Smirnov test was not conclusive, and we can point out that, for galactocentric distances smaller than 2.9 kpc, the α-elements abundances do not follow the disk radial gradient towards the center of the Milky Way galaxy.

5. SUMMARY AND CONCLUSION

This work reports an important result concerning PNe and the chemical evolution of the Galaxy. In addition to our previous work (Cavichia et al. 2010, Paper I), where we presented the chemical abundances and the analysis of these abundances for a sample of 56 PNe in the direction of the galactic bulge, among which 35 PNe have their abundances derived for the first time, we extended our data base to 140 PNe in order to study the chemical abundance distribution in the inner disk and bulge of the Galaxy.

In this work, a statistical analysis was performed in order to find the galactocentric distance where bulge and disk characteristics intersect. Two distance scales were used: Zhang (1995) and Stanghellini et al. (2008). Applying the Kolmogorov-Smirnov test, the former results in a distance of 1.5 kpc, while for the latter the test was not conclusive. Nevertheless, the radial α-elements abundance distributions for both scales indicate that they do not follow the trend of the disk. On average, the abundances for objects with galactocentric distances smaller than 1.5 and 2.2 kpc for the Z95 and SSV08 distance scales, respectively, are lower than for objects with distances greater than this limit, although this difference is not larger than the errors in individual abundances. Considering the SSV08 distance scale, the abundance difference between the two groups of PNe is based on 68, 62, 53, and 56 PNe of Group I (bulge) for O, S, Ar, and Ne, respectively, and 16, 15, 14, 12 PNe of Group II (inner disk) for the same elements. For the Z95 distance scale, the abundance difference is based on 72, 66, 50, and 43 PNe of Group I, and 41, 39, 28, 29 of Group II, for the same elements. Furthermore the combined error of the four elements (O, S, Ar, Ne) of each group is considerably smaller than the abundance difference between the two groups derived from the average difference of the four elements.

Taking into account the results derived in this work as well as other evidences from the literature, we propose the galactocentric distance of 1.5 kpc (for the Z95 distance scale) as the mark of the transition between the bulge and the inner-disk of the Galaxy.

Part of this work was supported by the Brazilian agencies *FAPESP* and *CNPq*. O.C. would like to acknowledge FAPESP for his graduate fellowship (processes 05/03194-4 and 07/07704-2). We also thank the referee for his/her comments and suggestions.

REFERENCES

Acker, A., Marcout, J., Ochsenbein, F., Stenholm, B., & Tylenda, R. 1992, Strasbourg-ESO Catalogue of Galactic Planetary Nebulae (Part 1 and 2; Garching: ESO)
Andrievsky, S. M., Luck, R. E., Martin, P., & Lépine, J. R. D. 2004, A&A, 413, 159
Binney, J. 2009, in IAU Symp. 254, The Galaxy Disk in Cosmological Context, ed. J. Andersen, J. Bland-Hawthorn, & B. Nordström (Cambridge: Cambridge Univ. Press), 145
Cahn, J. H., Kaler, J. B., & Stanghellini, L. 1992, A&AS, 94, 399 (CKS92)
Carigi, L., Peimbert, M., Esteban, C., & García-Rojas, J. 2005, ApJ, 623, 213
Cavichia, O., Costa, R. D. D., & Maciel, W. J. 2010, RevMexAA, 46, 159 (Paper I)
Chiappini, C., Górny, S., Stasińska, G., & Barbuy, B. 2009, A&A, 494, 591
Chiappini, C., Matteucci, F., & Romano, D. 2001, ApJ, 554, 1044
Costa, R. D. D., Escudero, A. V., & Maciel, W. J. 2005, in AIP Conf. Proc. 804, Planetary Nebulae as Astronomical Tools, ed. R. Szczerba, G. Stasińska, & S. K. Górny (Melville: AIP), 252
Costa, R. D. D., Maciel, W. J., & Escudero, A. V. 2008, Baltic Astron., 17, 321
Cuisinier, F., Maciel, W. J., Köppen, J., Acker, A., & Stenholm, B. 2000, A&A, 353, 543 (CMKAS00)
Cunha, K., Sellgren, K., Smith, V. V., Ramirez, S. V., Blum, R. D., & Terndrup, D. M. 2007, ApJ, 669, 1011
Daflon, S., & Cunha, K. 2004, ApJ, 617, 1115
Davies, B., et al. 2009, ApJ, 696, 2014
de Freitas Pacheco, J. A., Maciel, W. J., & Costa, R. D. D. 1992, A&A, 414, 211
Escudero, A. V., & Costa, R. D. D. 2001, A&A, 380, 300
Escudero, A. V., Costa, R. D. D., & Maciel, W. J. 2004, A&A, 414, 211
Exter, K. M., Barlow, M. J., & Walton, N. A. 2004, MNRAS, 349, 1291
Fu, J., Hou, J. L., Yin, J., & Walton, N. A. 2009, ApJ, 696, 668
Gerhard, O. 2002, in ASP Conf. Ser. 273, The Dynamics, Structure and History of Galaxies, ed. G. S. Da Costa & H. Jerjen (San Francisco: ASP), 73
Gillessen, S., Eisenhauer, F., Trippe, S., Alexander, T., Genzel, R., Martins, F., & Ott, T. 2009, ApJ, 692, 1075
Górny, S. K., Stasińska, G., Escudero, A. V., & Costa, R. D. D. 2004, A&A, 427, 231
Gutenkunst, S., Bernard-Salas, J., Pottasch, S. R., Sloan, G. C., & Houck, J. R. 2008, ApJ, 680, 1206
Henry, R. B. C., Kwitter, K. B., Jaskot, A. E., Balick, B., Morrison, M. A., & Milingo, J. B. 2010, ApJ, 724, 748
Hou, J. L., Prantzos, N., & Boissier, S. 2000, A&A, 362, 921
Howard, C. D., et al. 2009, ApJ, 702, L153
Köppen, J., Acker, A., & Stenholm, B. 1991, A&A, 248, 197
Maciel, W. J. 2000, in IAU Symp. 198, The Light Elements and their Evolution, ed. L. da Silva, R. De Medeiros, & M. Spite (San Francisco: ASP), 204
Maciel, W. J., Lago, L. G., & Costa, R. D. D. 2005, A&A, 433, 127
_________. 2006, A&A, 453, 587
Maciel, W. J., & Pottasch, S. R. 1980, A&A, 88, 1
Maciel, W. J., & Quireza, C. 1999, A&A, 345, 629
Milingo, J. B., Kwitter, K. B., Henry, R. B. C., & Souza, S. P. 2010, ApJ, 711, 619
Mishurov, Y. N., Lépine, J. R. D., & Acharova, I. A. 2002, ApJ, 571, L113
Mollá, M., & Díaz, A. I. 2005, MNRAS, 358, 521
Nishiyama, S., et al. 2006, ApJ, 647, 1093
Peimbert, M. 1978, in IAU Symp. 76, Planetary Nebulae, ed. Y. Terzian (Dordrecht: Reidel), 215
Peimbert, M., Luridiana, V., & Torres-Peimbert, S. 1995, RevMexAA, 31, 147
Perinotto, M., & Morbidelli, L. 2006, MNRAS, 372, 45
Perinotto, M., Morbidelli, L., & Scatarzi, A. 2004, MNRAS, 349, 793
Portinari, L., & Chiosi, C. 1999, A&A, 350, 827
_________. 2000, A&A, 355, 929
Ratag, M. A., Pottasch, S. R., Dennefeld, M., & Menzies, J. W. 1992, A&A, 255, 255
_________. 1997, A&AS, 126, 297
Rich, R. M. 1988, AJ, 95, 828
Rolleston, W. R. J., Smartt, S. J., Dufton, P. L., & Ryans, R. S. I. 2000, A&A, 363, 537
Ruffle, P. M. E., Zijlstra, A. A., Walsh, J. R., Gray, M. D., Gesicki, K., Minniti, D., & Comeron, F. 2004, MNRAS, 353, 796
Samland, M., Köppen, J., Acker, A., & Stenholm, B. 1992, A&A, 264, 184
Shen, J., Rich, R. M., Kormendy, J., Howard, C. D., De Propris, R., & Kunder, A. 2010, ApJ, 720, L72
Smartt, S. J., Venn, K. A., Dufton, P. L., Lennon, D. J., Rolleston, W. R. J., & Keenan, F. P. 2001, A&A, 367, 86

Stanghellini, L., & Haywood, M. 2010, ApJ, 714, 1096
Stanghellini, L., Shaw, R. A., & Villaver, E. 2008, ApJ, 689, 194 (SSV08)
Stasińska, G., Richer, M. G., & McCall, M. L. 1998, A&A, 336, 667
Tiede, G. P., & Terndrup, D. M. 1999, AJ, 118, 895
Tylenda, R., Siódmiak, N., Górny, S., Corradi, R. L. M., & Schwarz, H. E. 2003, A&A, 405, 627
Weiland, J. L., et al. 1994, ApJ, 425, L81
Zhang, C. Y. 1995, ApJS, 98, 659 (Z95)
Zoccali, M., et al. 2006, A&A, 457, L1
Zoccali, M., et al. 2003, A&A, 399, 931

O. Cavichia, R. D. D. Costa, and W. J. Maciel: Departamento de Astronomia, Instituto de Astronomia, Geofísica e Ciências Atmosféricas Universidade de São Paulo, Rua do Matão, 1226, Cidade Universitária, 05508-900 São Paulo-SP, Brazil (cavichia, roberto, maciel@astro.iag.usp.br).